This copy is for personal use only. To order printed copies, contact *reprints@rsna.org*

Imaging of Nonmalignant Adrenal Lesions in Children[1]

Kiran M. Sargar, MD
Geetika Khanna, MD, MS
Rebecca Hulett Bowling, MD

Abbreviations: ACTH = adrenocorticotropic hormone, CAH = congenital adrenal hyperplasia, EMH = extramedullary hematopoiesis, MIBG = metaiodobenzylguanidine

RadioGraphics 2017; 37:1648–1664

https://doi.org/10.1148/rg.2017170043

Content Codes: GU PD

[1]From the Mallinckrodt Institute of Radiology, Washington University School of Medicine, 510 S Kingshighway Blvd, Campus Box 8131-MIR, St Louis, MO 63110. Presented as an education exhibit at the 2016 RSNA Annual Meeting. Received March 8, 2016; revision requested April 24 and received May 10; accepted July 5. For this journal-based SA-CME activity, the authors, editor, and reviewers have disclosed no relevant relationships. Address correspondence to K.M.S. (e-mail: *kiran.sargar@gmail.com*).

©RSNA, 2017

SA-CME LEARNING OBJECTIVES

After completing this journal-based SA-CME activity, participants will be able to:

- List common pediatric nonmalignant adrenal lesions and adrenal lesion mimics and classify them based on their cause.
- Recognize the key clinical features and associations of nonmalignant adrenal lesions and adrenal lesion mimics in children.
- Identify distinguishing imaging findings of pediatric nonmalignant adrenal lesions and adrenal lesion mimics.

See www.rsna.org/education/search/RG.

The adrenal glands in children can be affected by a variety of benign lesions. The diagnosis of adrenal lesions can be challenging, but assessment of morphologic changes in correlation with the clinical presentation can lead to an accurate diagnosis. These lesions can be classified by their cause: congenital (eg, discoid adrenal gland, horseshoe adrenal gland, and epithelial cysts), vascular and/or traumatic (eg, adrenal hemorrhage), infectious (eg, granulomatous diseases), enzyme deficiency disorders (eg, congenital adrenal hyperplasia [CAH] and Wolman disease), benign neoplasms (eg, pheochromocytomas, ganglioneuromas, adrenal adenomas, and myelolipomas), and adrenal mass mimics (eg, extralobar sequestration and extramedullary hematopoiesis). Multimodality cross-sectional imaging helps to define the origin, extent, and relationship of these lesions to adjacent structures, as well as to guide treatment management. The anatomic and functional imaging modalities used to evaluate pediatric adrenal lesions include ultrasonography, computed tomography (CT), magnetic resonance imaging, and iodine 123 metaiodobenzylguanidine scintigraphy. Identifying the imaging features of nonmalignant adrenal lesions is helpful to distinguish these lesions from malignant adrenal neoplasms. Identifying characteristic imaging findings (eg, enlarged adrenal glands, with cerebriform surface, and stippled echogenicity in CAH; a T2-hyperintense mass with avid contrast enhancement in pheochromocytoma; low CT attenuation [<10 HU] and signal intensity drop on opposed-phase chemical shift images in adenoma; and enhancing suprarenal mass supplied by a systemic feeding artery in extralobar sequestration) can aid in making the correct diagnosis. In addition, clinical features (eg, ambiguous genitalia in CAH and hypertension in pheochromocytoma) can also guide the radiologist toward the correct diagnosis.

©RSNA, 2017 • *radiographics.rsna.org*

Introduction

Nonmalignant adrenal lesions are often seen in the pediatric population and encompass a set of peculiar characteristics. The Table classifies pediatric nonmalignant adrenal conditions based on their cause, including adrenal lesion mimics. The clinical manifestation of these lesions is often nonspecific, and diagnosis can be challenging.

TEACHING POINTS

- In infants, serial US is the imaging modality of choice for the evaluation of adrenal hemorrhage. Initially, adrenal hemorrhage is a well-defined slightly echo- to isoechoic mass; it may be homogeneous or heterogeneous. The lesion may involve only a portion of the adrenal gland, and a normal adrenal limb may be seen next to the hemorrhage. Because the mass is avascular, no internal flow is seen at color Doppler US.
- US of the adrenal gland is the modality of choice for the workup of CAH in neonates and infants. An adrenal gland with a limb length measurement of 20 mm or greater, mean width measurement of 4 mm or greater, and normal corticomedullary differentiation is suggestive of CAH. A combination of limb width greater than 4 mm, lobulated or cerebriform surface, and stippled echogenicity is highly sensitive and specific for the diagnosis of CAH.
- MR imaging is the modality of choice for the presurgical evaluation of pheochromocytomas. On MR images, pheochromocytomas show iso- to hypointense signal to muscle on T1-weighted images and markedly hyperintense signal ("light bulb sign") on T2-weighted images, with avid contrast enhancement. Up to 30% of pheochromocytomas show intermediate to low signal intensity on T2-weighted images or are heterogeneous secondary to internal hemorrhage or cystic degeneration.
- On nonenhanced CT images, low attenuation less than 10 HU is characteristic of lipid-rich adenomas. Lipid-poor adenomas show higher attenuation values. Calcifications are less common in adenomas than in adrenocortical carcinomas. At contrast-enhanced CT, adenomas show moderate homogeneous contrast enhancement with rapid washout at delayed imaging. At MR imaging, the lipid-rich adenomas show a signal intensity drop on opposed-phase chemical shift images, due to the presence of microscopic fat.
- Infradiaphragmatic extralobar sequestration may mimic an adrenal mass at imaging. Suprarenal extralobar sequestration may be seen as a well-defined radiopacity in the upper paraspinal region on chest and abdominal radiographs. US demonstrates a heterogeneous suprarenal mass, often pyramidal. The increased echogenicity is related to multiple tissue interfaces within the lesion. A thin and highly echogenic rim around the lesion may also be seen. The blood supply is from the aorta or branches of the aorta.

Multimodality cross-sectional imaging has a vital role for defining the origin, extent, and relationship of these lesions to adjacent structures, as well as guiding treatment management. The various anatomic and functional imaging modalities for the evaluation of pediatric adrenal lesions include ultrasonography (US), computed tomography (CT), magnetic resonance (MR) imaging, and iodine 123 (^{123}I) metaiodobenzylguanidine (MIBG) scintigraphy. Overall, US is the preferred initial imaging modality, and MR imaging is used as a problem-solving tool.

Knowledge of the imaging features of nonmalignant adrenal lesions is helpful to distinguish these lesions from malignant adrenal neoplasms. A constellation of characteristic imaging findings and certain clinical features are helpful in suggesting the correct diagnosis. The appropriate laboratory tests can be performed to confirm a particular diagnosis (eg, plasma-free metanephrine and normetanephrine for pheochromocytoma and serum 17-hydroxyprogesterone for congenital adrenal hyperplasia [CAH]).

In this article, we discuss the clinical manifestations and imaging findings of nonmalignant adrenal lesions that are common in the pediatric population. The key imaging findings that can aid the radiologist in making an accurate diagnosis are emphasized.

Normal Anatomy

The adrenal gland consists of paired endocrine glands located in the upper retroperitoneum. The right adrenal gland is located anterolateral to the right crus of the diaphragm, medial to the liver, and posterior to the inferior vena cava. The left adrenal gland is located medial to the upper pole of the left kidney, lateral to the left crus of the diaphragm, and posterior to the splenic vein and pancreas. The right adrenal gland is triangular, and the left adrenal gland is semilunar.

The adrenal cortex and medulla arise from separate embryologic structures. The adrenal cortex is mesodermal in origin and arises from the urogenital ridge. The adrenal medulla is ectodermal in origin and arises from neural crest tissue. The normal adrenal gland size is age dependent.

The adrenal gland can be visualized at obstetric US as early as 13–14 weeks gestation, at which time it is large, globular, and roughly 0.5 times the renal length. During late gestation, the adrenal gland size is about 0.3 times the renal length (1). In a neonate, the adrenal gland is more prominent when compared with the gland in an adult, and two limbs can be seen at US (2). The neonatal adrenal gland can have a slightly undulating contour, but the thickness of each limb should be less than 4 mm.

At US, the adrenal cortex and medulla are easily identifiable in a neonate (Fig 1) (2,3). The cortex is large and hypoechoic, while the medulla is small and hyperechoic in the newborn period. With increasing age, the cortex becomes smaller, the medulla becomes relatively larger, and the corticomedullary junction becomes less distinct by 5–6 months of age. After 1 year of age, the appearance of the adrenal gland is similar to that of an adult's, with straight or concave borders and a hypoechoic appearance.

The attenuation of the adrenal gland at CT is similar to that of the normal kidney. The signal intensity of the adrenal gland at MR imaging is similar to, or slightly less than, the signal intensity

RadioGraphics

of the liver (4). MR imaging sequences that best show adrenal anatomy are fat-suppressed T1-weighted and opposed-phase gradient-echo MR images (5). A normal adrenal gland shows avid enhancement on postcontrast images.

Accessory adrenal tissue, also known as *adrenal rest tissue*, can be found anywhere along the path of gonadal descent in the retroperitoneum. Accessory adrenal tissue is common in neonates and rarely seen in adults. It is most commonly seen in the regions of the celiac plexus, broad ligament of the uterus, ovaries, inguinal canal, testes, and epididymides.

Discoid Adrenal Gland

A discoid adrenal gland is so called because of its shape; it is also known as a *straight* or *pancake* adrenal gland. It is seen in association with congenital renal anomalies when the ipsilateral kidney is absent or ectopic, which results in an empty renal fossa (6). The presence of a kidney is required for the adrenal gland to attain a normal triangular or Y shape.

In the absence of normal upward pressure from the ipsilateral developing kidney, the adrenal gland has a "lying down" or discoid appearance (Fig 2). The normal echogenic medulla and surrounding hypoechoic cortex can still be seen and should not be mistaken for an atrophic kidney. No intervention is required for a discoid adrenal gland.

Horseshoe Adrenal Gland

A horseshoe adrenal gland is a rare congenital anomaly characterized by the fusion of the medial limbs of each adrenal gland. It is associated with asplenia syndrome (most common), neural tube defects, renal anomalies, and Cornelia de Lange syndrome (7–9).

Asplenia syndrome, also known as *right isomerism*, is characterized by bilateral trilobed lungs (Fig 3a), right atria, a horizontal midline liver, an absent spleen, malrotation, and congenital heart disease (8). Associated congenital heart anomalies in asplenia syndrome include total anomalous pulmonary venous return (most common), endocardial cushion defect, transposition of the great arteries, and pulmonic stenosis or atresia (10). The renal anomalies associated with a horseshoe adrenal gland are bilateral renal agenesis and horseshoe kidney.

US is useful for the evaluation of a horseshoe adrenal gland in neonates and infants. US demonstrates a solitary adrenal gland in the midline, with the fused portion passing anteriorly to the aorta (Figs 3b, 4a). CT and MR images (Fig 3c) show the fusion of the adrenal glands across the midline. A horizontal midline liver and an absent spleen are findings in patients with asplenia syndrome (Fig 3b, 3c). One should also look for the associated renal anomalies and spinal cord abnormalities (Fig 4b).

Most patients with a horseshoe adrenal gland do not have clinical or biochemical evidence of adrenal dysfunction (8). Associated abdominal, renal, cardiac, and spinal anomalies have to be addressed.

Classification of Nonmalignant Adrenal Conditions in Children

Category	Condition
Congenital	Discoid adrenal gland Horseshoe adrenal gland Epithelial cysts
Vascular and/or traumatic	Adrenal hemorrhage
Infectious	Granulomatous diseases
Enzyme deficiency disorders	CAH Wolman disease
Benign neoplasms	Pheochromocytoma Ganglioneuroma Adrenal adenoma Myelolipoma
Adrenal mass mimics	Extralobar sequestration EMH

Note.—CAH = congenital adrenal hyperplasia, EMH = extramedullary hematopoiesis.

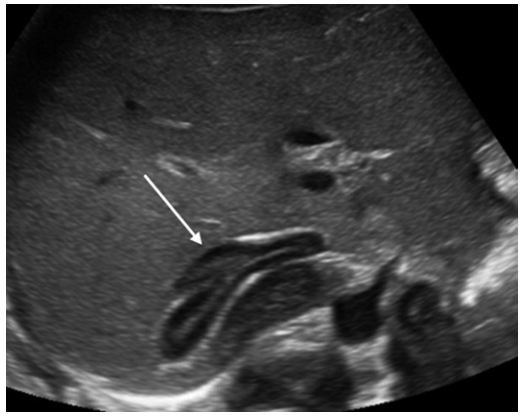

Figure 1. Normal right adrenal gland in a 1-day-old girl. Transverse US image of the right upper quadrant shows a normal right adrenal gland (arrow). Note the central echogenic medulla and peripheral hypoechoic cortex.

Adrenal Cysts

Adrenal cysts are rare lesions, especially in young children, and are found in less than 2% of autopsies (11). Nonneoplastic adrenal cysts have been classified into four groups: endothelial cysts (45%), pseudocysts (39%), epithelial cysts (9%), and parasitic cysts (7%) (12). Endothe-

RadioGraphics

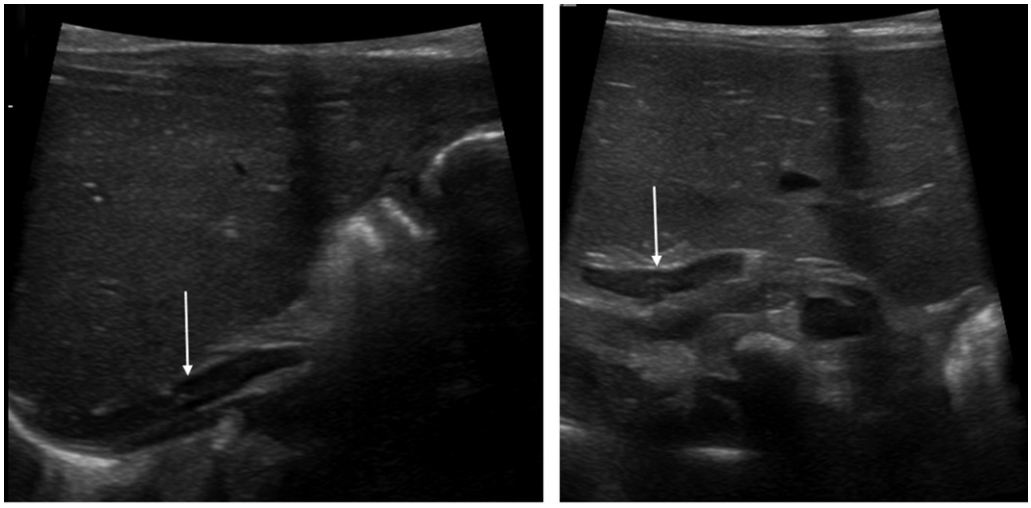

a. b.

Figure 2. Discoid right adrenal gland in a 1-day-old boy with an abnormal prenatal US examination. Longitudinal **(a)** and transverse **(b)** gray-scale US images of the right renal fossa show an absent right kidney with a flattened and elongated right adrenal gland (arrow).

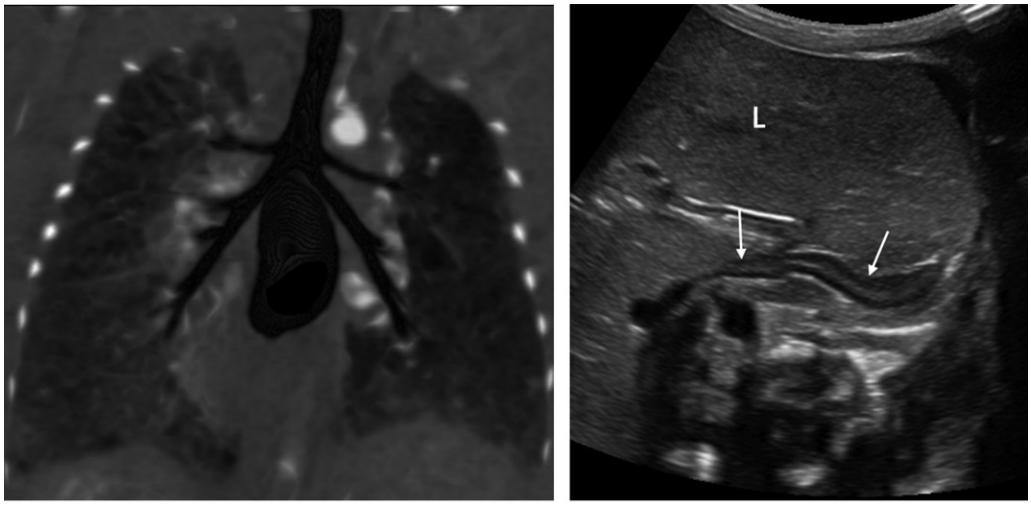

a. b.

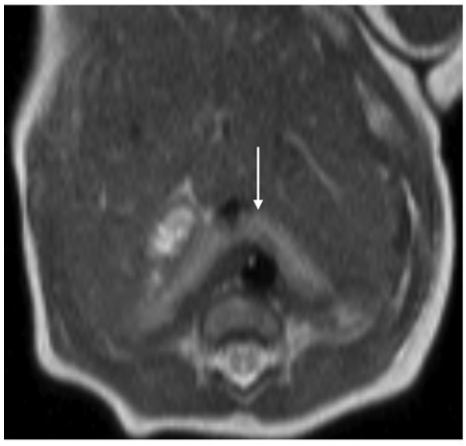

c.

Figure 3. Horseshoe adrenal gland in a 3-day-old boy with right isomerism (asplenia syndrome). **(a)** Coronal contrast material–enhanced CT image of the chest shows a bilateral right-sided bronchial branching pattern. **(b)** Transverse gray-scale US image of the upper abdomen shows a horseshoe adrenal gland (arrows), a midline liver *(L)*, and an absent spleen in the left upper quadrant. **(c)** Axial T2-weighted MR image of the upper abdomen shows a horseshoe adrenal gland (arrow) in the preaortic location and a midline liver and absent spleen in the left upper quadrant. These findings are most consistent with horseshoe adrenal gland in the setting of right isomerism.

lial cysts are further classified as lymphatic or angiomatous. Most pseudocysts in children are posthemorrhagic (13).

In most cases, adrenal cysts are small and incidentally found in asymptomatic patients (14). If a cyst becomes large, it may cause abdominal pain, vomiting, or a palpable mass. The symptoms may be acute if the cyst ruptures or becomes infected (15).

Adrenal cysts are usually not apparent on radiographs, as most are under 6 cm in diameter. Rarely,

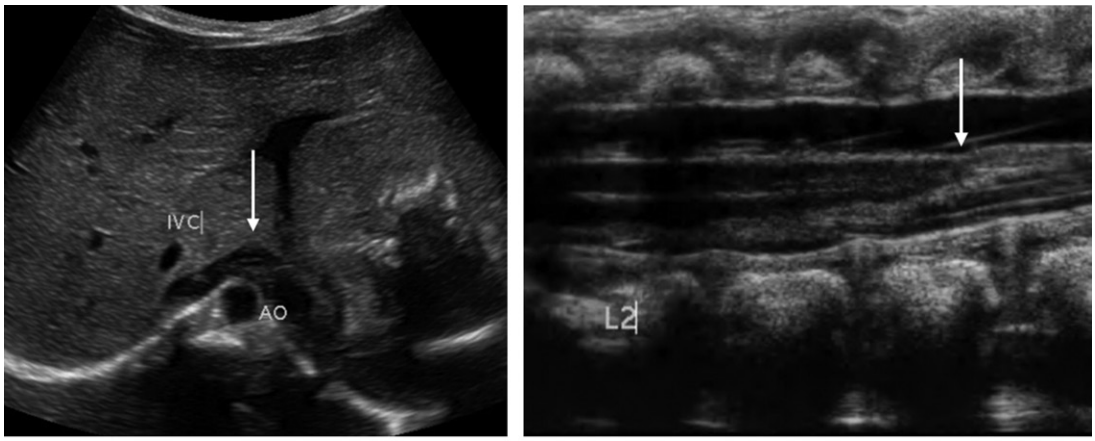

a. b.

Figure 4. Horseshoe adrenal gland in a 1-day-old boy with a tethered spinal cord. **(a)** Transverse gray-scale US image of the upper abdomen shows fusion of both adrenal glands (arrow) across the midline. *AO* = aorta, *IVC* = inferior vena cava. **(b)** Longitudinal spinal gray-scale US image shows a low-lying conus at the L4 through L5 levels (arrow).

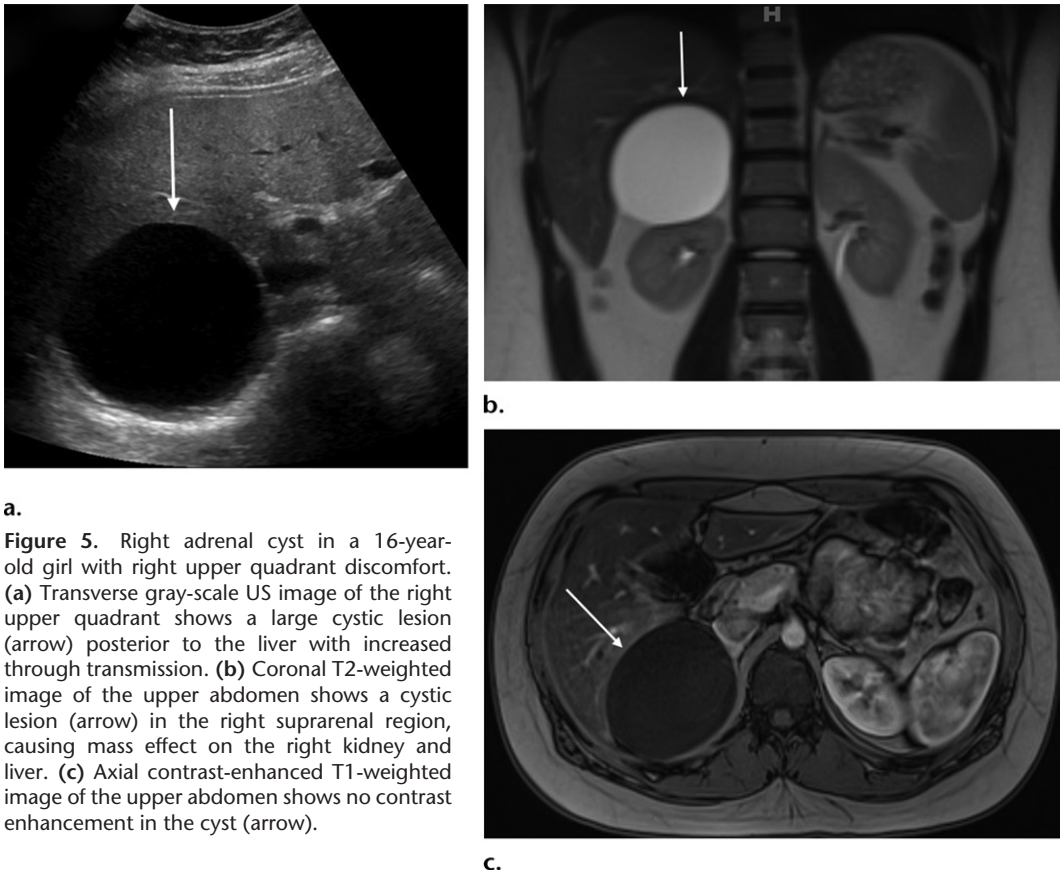

a. b. c.

Figure 5. Right adrenal cyst in a 16-year-old girl with right upper quadrant discomfort. **(a)** Transverse gray-scale US image of the right upper quadrant shows a large cystic lesion (arrow) posterior to the liver with increased through transmission. **(b)** Coronal T2-weighted image of the upper abdomen shows a cystic lesion (arrow) in the right suprarenal region, causing mass effect on the right kidney and liver. **(c)** Axial contrast-enhanced T1-weighted image of the upper abdomen shows no contrast enhancement in the cyst (arrow).

they may be large enough to cause mass effect on adjacent structures and be visible on abdominal radiographs (16). At US, true adrenal cysts are located in the suprarenal fossa and are typically round, well-defined, and anechoic, with through transmission and a thin wall (Fig 5a). They have no internal flow at color Doppler US (17).

With a lymphatic cyst, the wall may be lobulated, and thin septa may be seen. As with lymphatic malformations in other areas of the body, its flow may be demonstrated in the septa with color Doppler US. If calcifications or mural nodules are seen, then the lesion may be a pseudocyst or neoplasm. A pseudocyst may contain internal echoes related to blood products or show curvilinear rim echogenicity secondary to calcification.

Both endothelial-lined cysts and pseudocysts may contain peripheral nodular calcifications;

RadioGraphics

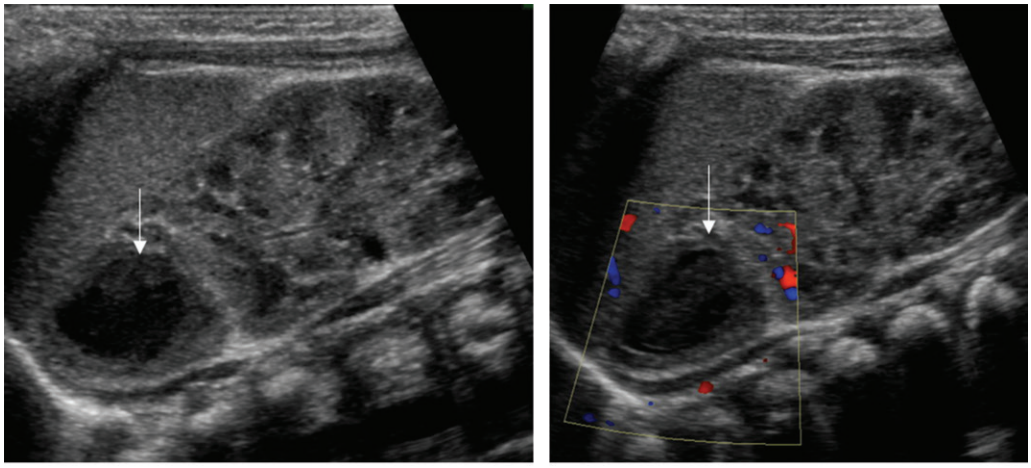

a. b.

Figure 6. Adrenal hemorrhage in an 8-day-old boy. Longitudinal gray-scale **(a)** and color Doppler **(b)** US images of the left upper abdomen show a mixed-echogenicity left suprarenal mass (arrow) with central hypoechoic and peripheral echogenic components. There is no appreciable color flow on the color Doppler US image. Follow-up US after 12 weeks showed complete resolution of adrenal hemorrhage (not shown).

central calcification has also been reported, which can be punctate or linear (18,19).

At MR imaging, simple cysts have low signal intensity on T1-weighted images and high signal intensity on T2-weighted images (Fig 5b). They have no soft-tissue components and do not enhance (Fig 5c) (20). Pseudocysts may have a variable appearance at MR imaging, depending on the components of the cyst. They may demonstrate septa, blood products, or hyaline thrombi (15).

Surgical resection is recommended for most adrenal cysts due to the difficulty in differentiating them from cystic neuroblastomas. US surveillance can be considered in select cases, especially if there is history supporting prior hemorrhage (11).

Adrenal Hemorrhage

An adrenal hemorrhage is the most common cause of an adrenal mass in a neonate, and it usually occurs in the first few days of life. In the newborn period, adrenal hemorrhage occurs in two of 1000 patients, and they are nearly four times more common than neuroblastomas (21). Ten percent of adrenal hemorrhage cases are bilateral, and 70% are on the right side (22). The reason for the right side preponderance is unclear, although one theory suggests that this is due to the compression of the right adrenal gland between the liver and right kidney. It is thought that the large size and increased vascularity of the neonatal adrenal gland may predispose the gland to hemorrhage.

An adrenal hemorrhage may be incidentally detected in a neonate at US. It more commonly occurs in a neonate with a history of difficult delivery or birth trauma, sepsis, perinatal hypoxia, or a bleeding diathesis. The clinical presentation is variable and includes a palpable mass, anemia, jaundice, abdominal pain, and/or shock. Adrenal hemorrhage can be secondary to renal vein thrombosis, in which case it is more common on the left side. This is likely because the left adrenal vein drains into the renal vein, while the right adrenal vein drains directly into the inferior vena cava.

Renal vein thrombosis and adrenal hemorrhage are more common in the infants of diabetic mothers. Adrenal hemorrhage can also be seen in approximately 1% of children in the setting of blunt abdominal trauma, often in association with other visceral injuries (23). Severe bilateral adrenal hemorrhage can occur in Waterhouse-Friderichsen syndrome, which can result in adrenal insufficiency (24).

Adrenal hemorrhage has a variable appearance, depending on the age of the hemorrhage and the patient's age (25). Adrenal hemorrhage is usually not seen on radiographs, unless the hematoma is large enough to cause mass effect and/or contains calcifications.

In infants, serial US is the imaging modality of choice for the evaluation of adrenal hemorrhage. Initially, adrenal hemorrhage is a well-defined slightly echo- to isoechoic mass; it may be homogeneous or heterogeneous. The lesion may involve only a portion of the adrenal gland, and a normal adrenal limb may be seen next to the hemorrhage (26). Because the mass is avascular, no internal flow is seen at color Doppler US (Fig 6b).

A neuroblastoma can appear with characteristics similar to those of an adrenal hemorrhage in up to 50% of cases and is the main differential

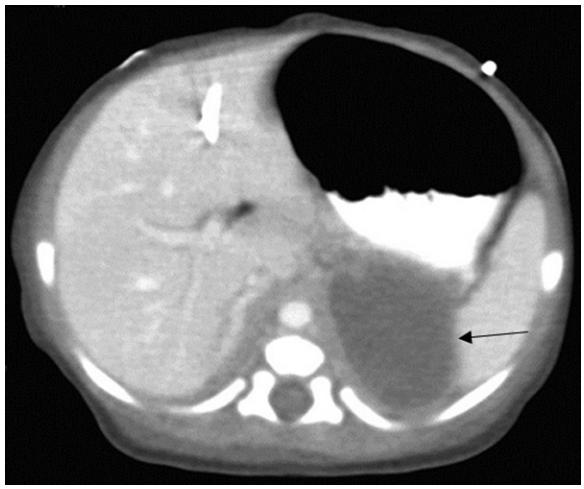

Figure 7. Left adrenal hemorrhage in the setting of renal vein thrombosis in a 1-day-old boy with abdominal distention. Axial contrast-enhanced CT image shows a nonenhancing hypoattenauting lesion (arrow) in the left suprarenal region. The adrenal hemorrhage resolved at follow-up imaging (not shown).

diagnosis (26). Because a neonatal neuroblastoma generally has a favorable outcome, it is recommended that short-term follow-up US be performed (14).

With serial scanning, an adrenal hemorrhage will show cystic transformation and involution (27). In infants with adrenal hemorrhage secondary to renal vein thrombosis, gray-scale US images of the kidney may show multiple hyperechoic linear streaks that represent thrombosed intrarenal veins, with no flow on color Doppler US images.

As liquefaction occurs, the mass becomes more complex, often with a central hypoechoic area (Fig 6a). Over time, the hemorrhage may become completely cystic, without internal echoes (28). If the hemorrhage calcifies, the periphery may show punctate or curvilinear areas of echogenicity. Calcification can occur as early as 1–2 weeks (22). Eventually, the hemorrhage resolves, and the adrenal gland resumes a normal size and shape.

As with US, the CT and MR imaging appearances of an adrenal hemorrhage are dependent on the age of the hemorrhage. A rounded nonenhancing suprarenal mass (Fig 7) may be seen with or without focal preservation of normal adrenal enhancement. The size of the hemorrhage is variable (29).

The CT attenuation is typically about 50–90 HU (25), and periadrenal fat stranding may be seen (29). The lesion will usually become smaller and less attenuated over time. An organized chronic hematoma appears as a round or oval mass with a low-attenuation center. The wall is usually thicker than that of an adrenal cyst. Calcifications may or may not be present. If present, they are often in the periphery and are termed *adrenal pseudocysts*. The absence of enhancement confirms that the mass is cystic (22). Complete resolution may occur, usually over the course of several weeks (29).

MR imaging (Fig 8a, 8b) can be used as a problem-solving tool to distinguish a hemorrhage from a neuroblastoma; however, follow-up is essential to exclude a hemorrhagic/cystic neuroblastoma. In the acute stage, adrenal hemorrhage is isointense or slightly hypointense on T1-weighted images and markedly hypointense on T2-weighted images, due to a high concentration of intracellular deoxyhemoglobin.

In the subacute stage, adrenal hemorrhage is hyperintense on T1- and T2-weighted images, due to the paramagnetic effects of free methemoglobin. There is blooming (loss of signal) on T2-weighted gradient-echo (T2*-weighted) images. In the chronic stage, a dark rim is present on T1- and T2-weighted images, secondary to hemosiderin deposition and the presence of a fibrous capsule.

Most cases of adrenal hemorrhage resolve without clinical sequelae. In cases of severe bilateral adrenal hemorrhage with resulting adrenal insufficiency, glucocorticoid (possibly mineralocorticoid) replacement therapy and androgen therapy are necessary.

Adrenal Calcifications

Adrenal calcifications carry a broad differential diagnosis and commonly occur as a sequel of prior adrenal hemorrhage or old granulomatous infections, such as histoplasmosis and tuberculosis (7,30). Rarely, viral infections of childhood, such as disseminated neonatal herpes simplex and cytomegalovirus infections, may cause calcifications (7). Wolman disease is a rare autosomal recessive disorder with acid lipase deficiency that causes adrenal gland calcifications. In addition, lipid deposition is seen in the liver, adrenal gland, spleen, and lymph nodes in patients with Wolman disease (31).

Adrenal calcification may be seen as radiopaque foci in the suprarenal region on abdomi-

RadioGraphics

Figure 8. Adrenal hemorrhage in a fetus at 34 weeks gestation. **(a, b)** Sagittal T2-weighted **(a)** and T1-weighted **(b)** MR images show a T2-hyperintense lesion (arrow in **a**) in the left suprarenal location, which is mildly T1 hyperintense (arrow in **b**) suggesting blood products. A layering debris level is seen on the T2-weighted image. This lesion measured 3 cm in maximum diameter. **(c)** Follow-up longitudinal gray-scale US image at birth shows evolving left adrenal hemorrhage (arrow), which decreased to 2 cm in maximum dimension. There was resolution of adrenal hemorrhage at subsequent follow-up imaging (not shown).

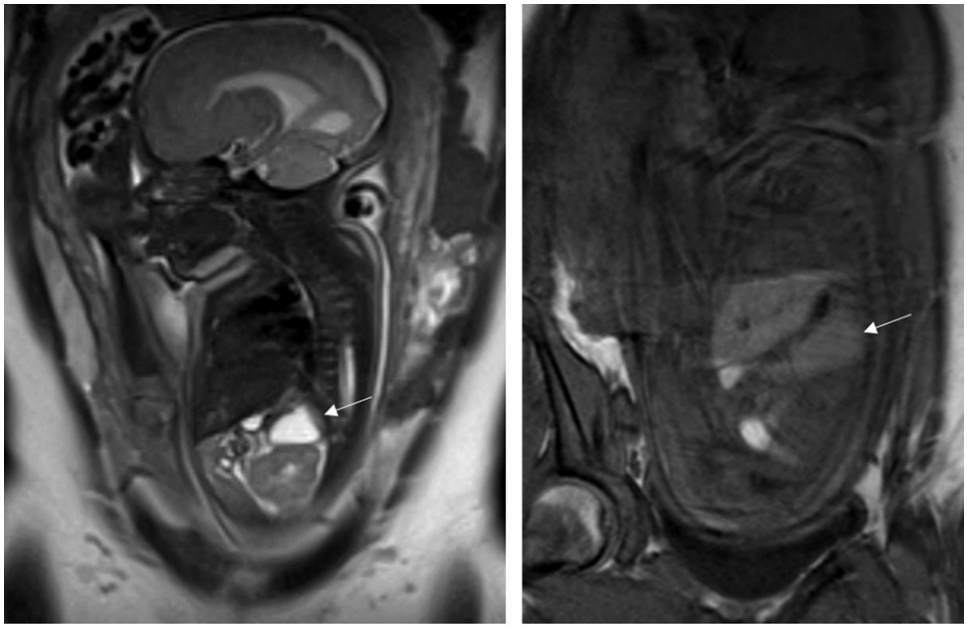

a. **b.**

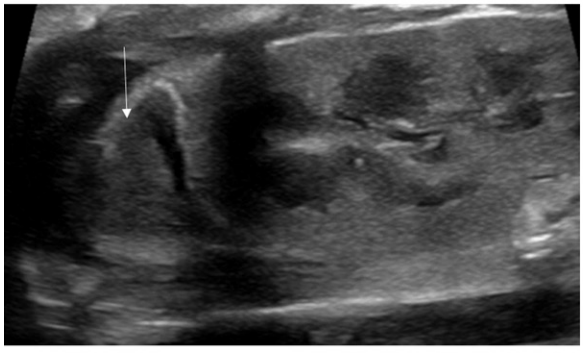

c.

nal radiographs, unilateral or bilateral. At US, calcifications are seen as echogenic foci with posterior acoustic shadowing. Small or punctate foci of calcification may not show posterior acoustic shadowing.

CT is sensitive for the detection of adrenal calcifications, which are seen as hyperattenuating foci (Fig 9). Adrenal calcifications are difficult to depict on conventional MR images. MR imaging T2*-weighted sequences may show adrenal calcifications as foci of low signal intensity due to magnetic susceptibility.

Although adrenal calcifications are nonspecific, the pattern of calcifications may be useful to suggest an underlying cause. Adrenal hemorrhage typically results in coarse and irregular calcification in a normal-sized or atrophic gland. Prior granulomatous infections, such as histoplasmosis or tuberculosis, typically show bilateral, small, faint, and diffuse calcifications at imaging in a normal-sized or atrophic gland (7,30).

If there is a mass associated with adrenal calcifications, various benign and malignant neoplasms should be considered. Peripheral curvilinear calcification may be seen in adrenal pseudocysts (30). In Wolman disease, the adrenal glands are enlarged with bilateral dense punctate calcifications and maintain an adreniform shape (7,30). CT images may show hepatosplenomegaly, bowel wall thickening, and enlarged low-attenuation lymph nodes secondary to fat deposition (7,31). At MR imaging, the adrenal gland may show hyperintense signal on T1- and T2-weighted images due to the increased lipid content (31).

Chronic granulomatous infections may result in adrenal insufficiency (Addison disease), due to significant gland destruction (7,30).

Congenital Adrenal Hyperplasia

CAH, also known as *adrenogenital syndrome*, is an autosomal recessive inborn error of metabolism due to a deficiency of the enzymes required for cortisol and aldosterone synthesis in the adrenal cortex (32). A 21-hydroxylase deficiency is the most common cause (90%–95% of cases),

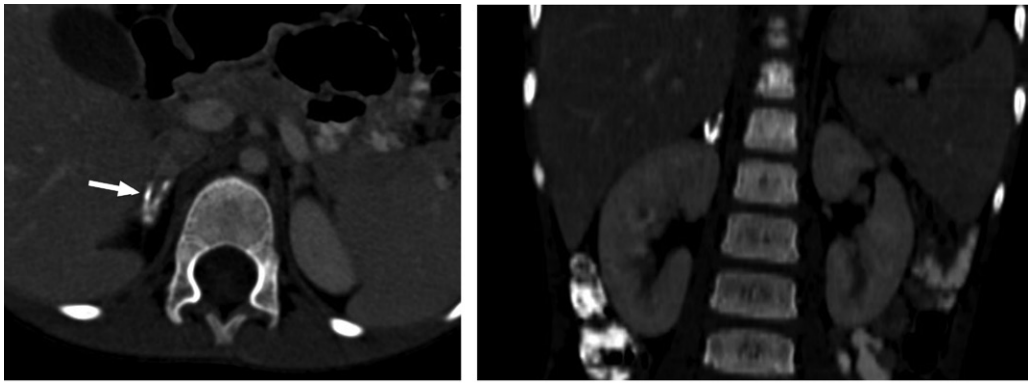

a. b.

Figure 9. Right adrenal calcification incidentally noted in a 5-year-old boy. Axial **(a)** and coronal **(b)** contrast-enhanced CT images of the abdomen show a V-shaped linear hyperattenuating lesion in the right suprarenal region (arrow in **a**), consistent with right adrenal calcification. There is no associated mass. This may represent sequelae of prior trauma.

which is due to an inactivating mutation of *CYP21A2* (32,33).

A less common cause of CAH is an 11-β-hydroxylase deficiency, which also manifests with masculinizing features (32,33). Inadequate cortisol synthesis leads to pituitary overproduction of adrenocorticotropic hormone (ACTH), due to an abnormal negative feedback mechanism. Excessive ACTH causes stimulation and hyperplasia of the adrenal cortex, with increased production of steroid precursors. The excess steroid precursors are converted into androgens. This results in masculinization of the external genitalia.

Girls with CAH due to 21-hydroxylase deficiency present in the perinatal period with ambiguous external genitalia (clitoral hypertrophy and labioscrotal fold enlargement), and boys present with isosexual precocious puberty. CAH is the most common cause of ambiguous genitalia in girls (34). There is decreased synthesis of aldosterone in the majority of these patients (approximately 75% of cases), leading to an acute life-threatening salt-wasting crisis due to hyponatremia, hypokalemia, and hypotension (32,35). Salt-wasting crisis is common in the first days to weeks of life, typically at 1–4 weeks (32,35). An early diagnosis of CAH is essential to assign the correct sex in girls with ambiguous genitalia and to prevent a potentially life-threatening salt-wasting crisis.

Excessive ACTH secretions may lead to hyperplasia of adrenal cortical rests in the testes in boys with CAH and form testicular adrenal rest tumors, also known as *testicular adrenal rests*. This explains the high prevalence of testicular adrenal rest tumors in males with CAH. These tumors are histologically similar to Leydig cell tumors; however, unlike Leydig cell tumors, these are usually bilateral (32). Testicular adrenal rest tumors are common in postpubertal boys with CAH and are usually small and multiple (32).

US of the adrenal gland is the modality of choice for the workup of CAH in neonates and infants (35,36). An adrenal gland with a limb length measurement of 20 mm or greater, mean width measurement of 4 mm or greater, and normal corticomedullary differentiation is suggestive of CAH (Fig 10a, 10b) (34,37). A combination of limb width greater than 4 mm, lobulated or cerebriform surface, and stippled echogenicity is highly sensitive and specific for the diagnosis of CAH (Fig 10a, 10b) (36).

A normal-sized adrenal gland does not exclude the diagnosis of CAH (34,37). The cerebriform appearance of the adrenal gland is thought to be specific (35,36). US is also useful to demonstrate normal uteri and ovaries in girls with ambiguous genitalia. Genitography demonstrates normal cervical indentation on the contrast material–filled vagina in girls with CAH (Fig 10c). CT images may show bilateral symmetric enlargement of the adrenal gland, with maintained shape and attenuation. Similarly, MR imaging may show an enlarged adrenal gland with normal signal intensity.

US of testicular adrenal rests shows bilateral multifocal intratesticular masses of varying sizes, which are commonly located near the mediastinum testis (Fig 11) (32,38). The small lesions typically appear hypoechoic compared with normal testicular tissue, while larger lesions may appear hypoechoic with internal hyperechoic reflections (32,38). At color Doppler US, these masses are predominantly avascular to hypovascular (Fig 11) (39).

At MR imaging, adrenal rests in a testicle are isointense to slightly hyperintense on T1-weighted images and hypointense on T2-weighted images when compared with the

RadioGraphics

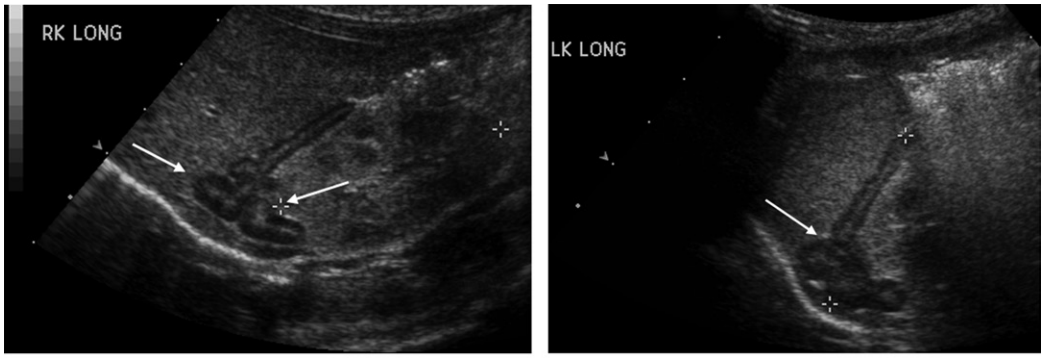

a. b.

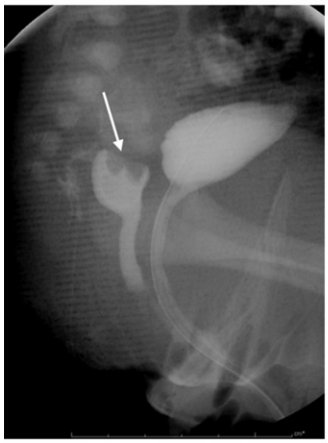

c.

Figure 10. CAH in a 1-day-old girl with ambiguous genitalia. **(a, b)** Longitudinal gray-scale US images of the right **(a)** and left **(b)** renal fossae show enlarged cerebriform adrenal glands (arrows) with limb thickness at 5 mm, compatible with CAH. **(c)** Lateral genitogram shows cervical indentation (arrow) on the contrast material–filled vagina.

adjacent testicle (32,38,39). On postcontrast T1-weighted images, these masses show diffuse contrast enhancement (39).

An elevated 17-hydroxy-progesterone serum level indicates the diagnosis of CAH (33,34). The 11-deoxycortisol and deoxycorticosterone levels are elevated in patients with 11-β-hydroxylase deficiency and low in patients with 21-hydroxylase deficiency (33). Glucocorticoid and mineralocorticoid replacement therapy is the treatment of choice for classic CAH due to 21-hydroxylase deficiency; however, these patients are prone to developing the long-term effects of steroid therapy (eg, decreased bone mineral density, early skeletal maturation and short stature, obesity, and impaired fertility). Testicular adrenal rest tumors are benign and will stabilize or regress with glucocorticoid therapy.

Pheochromocytoma

Pheochromocytoma, also known as an *intra-adrenal paraganglioma*, is a tumor that arises from catecholamine-producing chromaffin cells of the adrenal medulla. Although pheochromocytoma is less common in children than in adults, it is the most common pediatric endocrine neoplasm (40). It usually manifests in young adolescents, with a mean age of 11 years, and is more common in boys, with a male-to-female ratio of 2:1 (40,41).

The formerly used "10% rule" has been challenged. According to the 10% rule, 10% of the pheochromocytomas are hereditary. In children, approximately 40% of pheochromocytomas are associated with known genetic mutations, 8%–43% are extra-adrenal, and 19%–38% are bilateral adrenal (40). Multiple tumors may be seen in 30%–70% of cases, especially in those with a familial predisposition (14).

Pheochromocytomas occur in von Hippel–Lindau syndrome, multiple endocrine neoplasia syndrome type 2, neurofibromatosis type 1, and familial paraganglioma syndromes (40). Familial paraganglioma syndromes are caused by mutations in the succinate dehydrogenase *(SDH)* gene (40). Whole-body MR imaging is recommended in patients with an *SDH* gene mutation, in addition to biochemical screening (42).

Extra-adrenal pheochromocytomas, more appropriately known as *paragangliomas*, occur along the sympathetic chain from the skull base to the pelvis. The most common location of extra-adrenal paragangliomas in children is the upper retroperitoneum (14,41). Adrenal pheochromocytomas and intra-abdominal paragangliomas are usually hormonally active and produce epinephrine, norepinephrine, and vasoactive intestinal peptide (40,41). The resultant symptoms include hypertension (most common), palpitations, sweating, headaches, blurred vision, flushing, diarrhea, and weight loss (41).

In contrast, head and neck paragangliomas rarely produce substantial amounts of catecholamines (40,41). The first step in patients with a suspected pheochromocytoma is to perform biochemical testing, with quantification of plasma-free metanephrine and normetanephrine levels or measurement of 24-hour urinary fractionated metanephrine level (40).

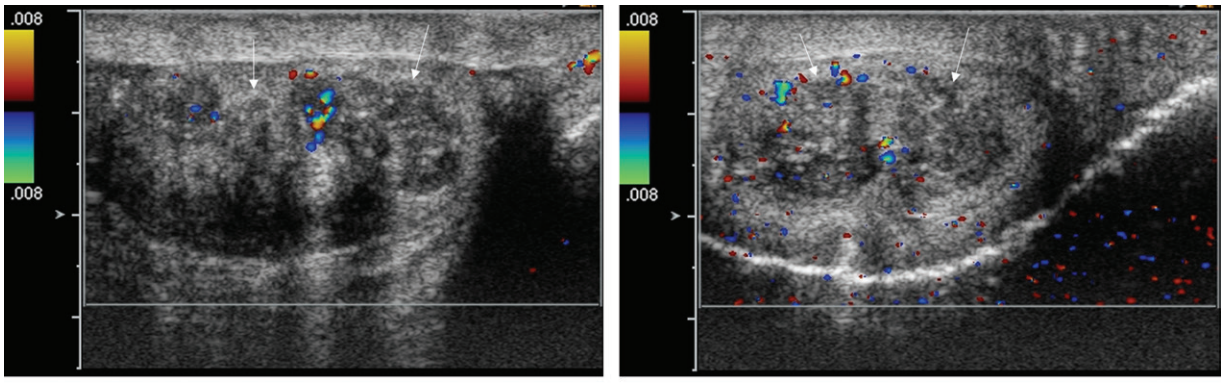

a. b.

Figure 11. Testicular adrenal rests in a 15-year-old boy with CAH. Longitudinal color Doppler US images of the right **(a)** and left **(b)** testes show bilateral multifocal heterogeneous intratesticular masses with mild internal vascularity (arrows).

At histologic analysis, pheochromocytomas are shown to be composed of nests or cords of polyhedral cells, separated by a fibrovascular stroma. Even though malignant features (eg, nuclear pleomorphism, necrosis, mitoses, and capsular and vascular invasion) may be seen in some tumors, they do not correlate with malignant behavior. The diagnosis of malignancy is usually based on the presence of extensive local invasion and metastatic disease (41,43).

US can be used for the evaluation of suspected pheochromocytomas in children (14). At US, a pheochromocytoma is seen as a suprarenal soft-tissue mass, which is iso- to hypoechoic to the liver, with increased vascularity at color Doppler US (Fig 12a). Contrast-enhanced CT images demonstrate a hypoattenuating suprarenal mass that shows intense contrast enhancement. Small tumors (<3 cm) show homogeneous contrast enhancement. Larger masses may have a heterogeneous appearance due to intratumoral hemorrhage and cystic degeneration (17). A small number of cases of pheochromocytoma may show calcification. There is no adverse risk with the use of nonionic contrast material in patients with pheochromocytoma, and the routine use of adrenergic blockade to prevent a hypertensive crisis is not necessary (14,17,44).

MR imaging is the modality of choice for the presurgical evaluation of pheochromocytomas (41). On MR images, pheochromocytomas show iso- to hypointense signal to muscle on T1-weighted images and markedly hyperintense signal ("light bulb sign") on T2-weighted images (Fig 12b), with avid contrast enhancement (Fig 12c) (7,14,44). Up to 30% of pheochromocytomas show intermediate to low signal intensity on T2-weighted images or are heterogeneous secondary to internal hemorrhage or cystic degeneration (Fig 12c) (17,30). One should look for local invasion into the adjacent structures and distant metastases, as these are the only reliable imaging findings for the diagnosis of malignant pheochromocytoma. The most common sites of metastatic disease are the bones, liver, lymph nodes, and lungs (7).

Functional imaging at ^{123}I-MIBG scintigraphy shows increased uptake in the tumor. It is useful for the evaluation of bilateral, multifocal, or metastatic disease (14,40). Given the high prevalence of hereditary pheochromocytomas in children, ^{123}I-MIBG scintigraphy is essential for the evaluation of multifocal disease before surgery (14,40). ^{123}I-MIBG scintigraphy is not specific for pheochromocytomas; other tumors (eg, neuroblastomas, ganglioneuroblastomas, and ganglioneuromas) also show increased MIBG uptake.

Surgical resection is the mainstay of pheochromocytoma treatment in children, and preoperative medical treatment is necessary to block the effects of intraoperative release of catecholamines due to tumor manipulation (40,41). Surgical resection is curative for benign tumors, and most pheochromocytomas in the pediatric population are benign. Because approximately 40% of pheochromocytomas in children have a hereditary basis, proper genetic testing should be performed.

Ganglioneuroma

A ganglioneuroma is a primary neural crest neoplasm of sympathetic nerve origin, which most commonly arises from the posterior mediastinum or retroperitoneum (45). Other locations include the adrenal gland, skin, tongue, appendix, and lymph nodes (45). Ganglioneuromas occur in the adrenal glands in 21% of cases (46). It is the most mature and benign form of the neural crest cell tumors. It contains mature ganglion cells and encapsulated nerve fibers, but it does not contain neuroblasts or increased mitotic figures (17).

RadioGraphics

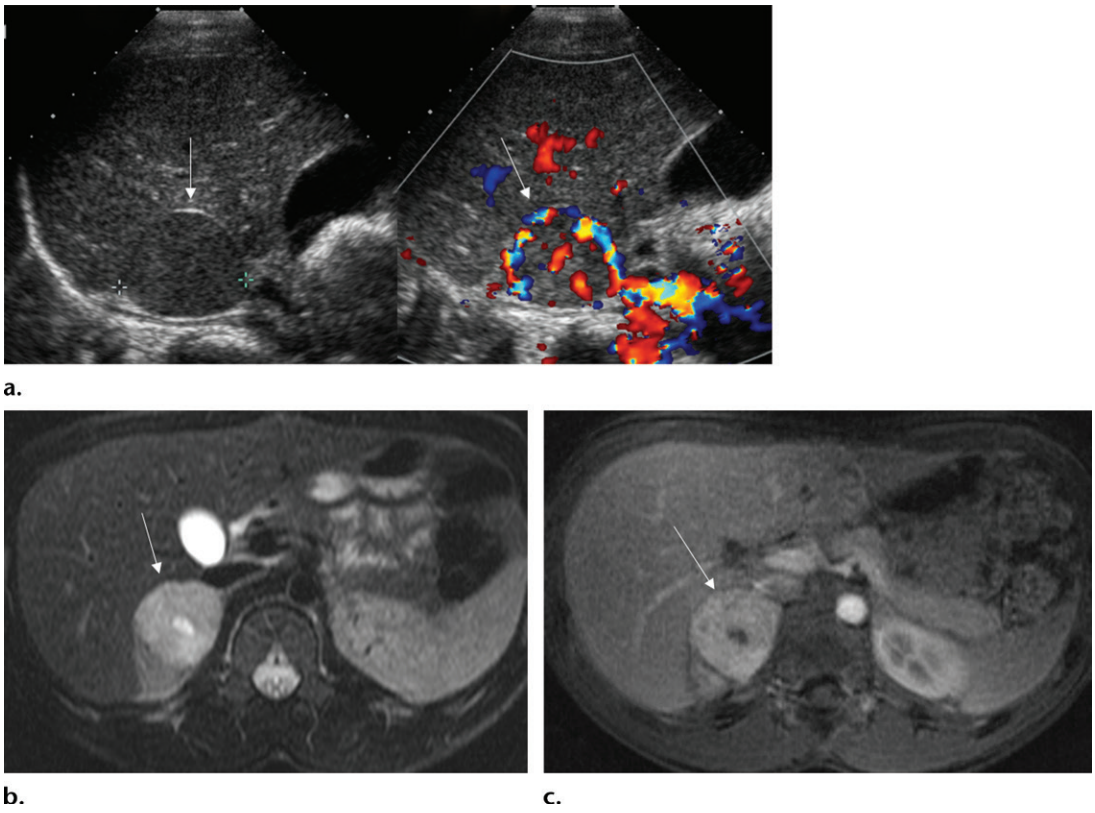

Figure 12. Pheochromocytoma in a 12-year-old boy with headaches, vomiting, and poorly controlled hypertension. **(a)** Transverse gray-scale (left) and color Doppler (right) US images of the upper abdomen show a well-defined hypoechoic right suprarenal mass (arrow) with intense internal vascularity. **(b, c)** Axial fat-suppressed T2-weighted **(b)** and axial fat-suppressed T1-weighted postcontrast **(c)** MR images show an enhancing T2-hyperintense right adrenal mass (arrow) with a central nonenhancing cystic or necrotic component.

Ganglioneuromas usually occur in older children, with a median age of 7 years at diagnosis. In one study, ganglioneuromas were found to be more common in girls, whereas neuroblastomas were more common in boys, with a peak age of under 3 years (47). The patient is often asymptomatic, and the mass may be found incidentally, even when large. If there is local mass effect, symptoms include cough, dyspnea, or pain (48). If there is spinal canal involvement, neurologic symptoms can occur. Rarely, ganglioneuromas can produce enough vanillylmandelic acid or homovanillic acid to cause flushing or other symptoms of catecholamine excess (49).

At US, the suprarenal mass is homogeneously hypoechoic and well circumscribed. Less commonly, the mass can be slightly heterogeneous (50). Extension across the midline can occur (51). Portions of a normal adrenal gland may be seen adjacent to the mass. Small calcifications may be seen as echogenic foci within the mass but are better demonstrated at CT.

At CT, the mass is well-defined with homogeneous low attenuation, similar to or slightly less attenuated than muscle (Fig 13a, 13b) (52). There is usually mild enhancement after intravenous contrast material administration. The enhancement may be homogeneous or heterogeneous (Fig 13a, 13b) (46). About 50% of ganglioneuromas demonstrate calcification at CT (17). The calcifications are more often small and punctate, unlike the more coarse calcifications typically seen in a neuroblastoma (53).

At MR imaging, a ganglioneuroma is well-defined, with low signal intensity on T1-weighted images and heterogeneous intermediate to high signal intensity on T2-weighted images (Fig 13c). It shows variable enhancement after intravenous contrast material administration (Fig 13d). A fibrous pseudocapsule is sometimes seen, which has low signal intensity on T1- and T2-weighted images (14). Delayed postcontrast images may show increasing enhancement (47). MR imaging is also the best modality to assess for intraspinal extension of the lesion (52).

Ganglioneuromas show increased uptake at ^{123}I-MIBG scintigraphy, similar to neuroblastomas and ganglioneuroblastomas. A few case reports have shown that ganglioneuromas can show variable fluorodeoxyglucose (FDG) uptake at FDG positron emission tomography (PET)/CT. The role of FDG PET/CT to distinguish

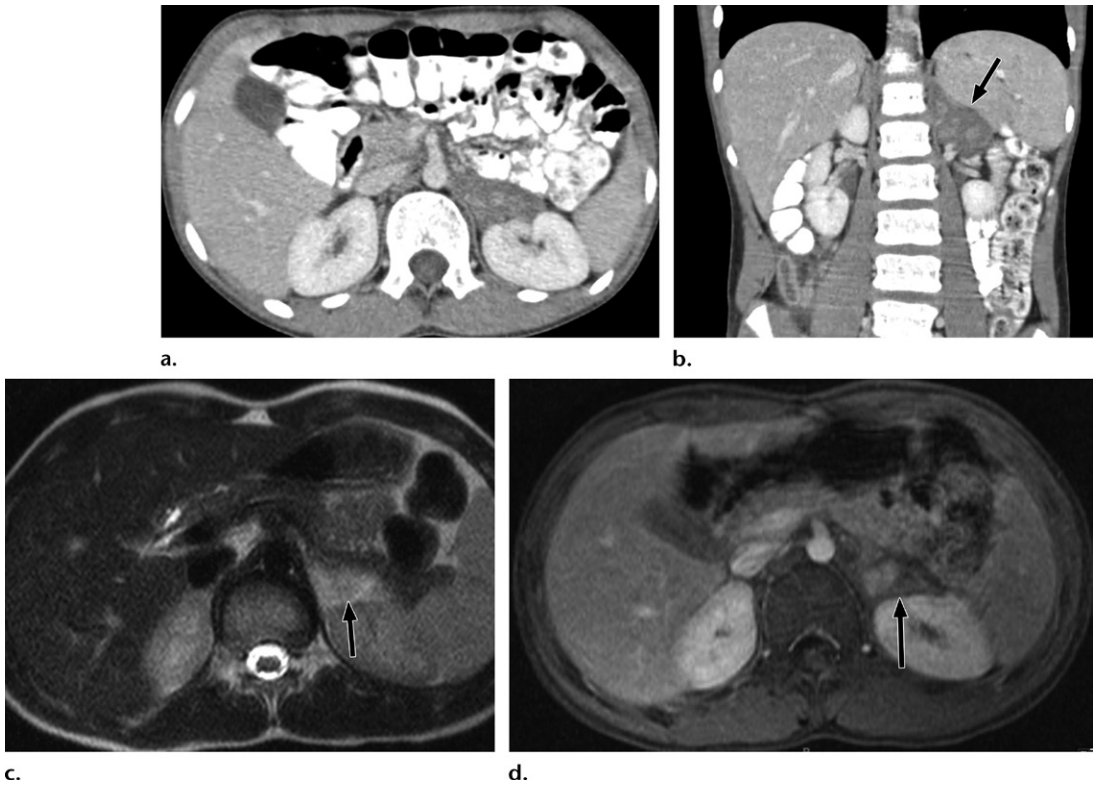

Figure 13. Adrenal ganglioneuroma in a 12-year-old boy with abdominal pain. **(a, b)** Axial **(a)** and coronal **(b)** contrast-enhanced CT images of the abdomen show a hypoattenuating left adrenal mass (arrow in **b**) with mild heterogeneous enhancement. **(c, d)** Axial T2-weighted **(c)** and axial fat-suppressed T1-weighted postcontrast **(d)** MR images of the abdomen show a T2-hyperintense left adrenal mass (arrow) with mild heterogeneous contrast enhancement.

between ganglioneuromas and neuroblastomas is unclear.

Ganglioneuromas can mimic the most malignant form of the neural crest cell tumors—neuroblastomas. Pathologic analysis is required to make the diagnosis. The treatment is surgical excision, when possible.

Adrenal Adenoma

An adrenal adenoma is a benign neoplasm that arises from the adrenal cortex, most commonly from the zona fasciculata (54). Adrenocortical adenomas are rare in children and less common than adrenocortical carcinomas (55,56). Adrenal adenomas are more common in children under 5 years of age or over 10 years of age, and they are more common in girls than boys (55). In contrast to adenomas in adults, adenomas in children are often hormonally active and manifest with peripheral precocious puberty, virilization, Cushing syndrome, hypertension, and feminization (55–57). Adrenal adenomas manifesting as an incidentally detected adrenal mass at imaging are uncommon in the pediatric population.

At histologic analysis, adenomas show cells arranged in nests separated by a fibrovascular stroma. The cytologic features include large pale vacuolated cells, with vesicular nuclei resembling normal zona fasciculata or small cells with eosinophilic cytoplasm and condensed chromatin, similar to a normal zona reticularis (58). It is difficult to separate adenomas from adrenocortical carcinomas; the histologic features that suggest malignancy are capsular invasion, vascular invasion, tumor necrosis, increased mitotic activity, and the presence of atypical mitotic figures (54,55). Biochemical analysis in patients with adenomas shows elevated serum and urinary levels of androstenedione, dehydroepiandrosterone sulfate, testosterone, and steroids (44).

At US, an adenoma appears as a well-circumscribed round or oval mass, with variable internal vascularity at color Doppler US (Fig 14a) (17). On nonenhanced CT images, low attenuation less than 10 HU is characteristic of lipid-rich adenomas (17,30). Lipid-poor adenomas show higher attenuation values. Calcifications are less common in adenomas than in adrenocortical carcinomas (7,57,58).

At contrast-enhanced CT, adenomas show moderate homogeneous contrast enhancement with rapid washout at delayed imaging (17). At MR imaging, the lipid-rich adenomas show a signal intensity drop on opposed-phase chemical

RadioGraphics

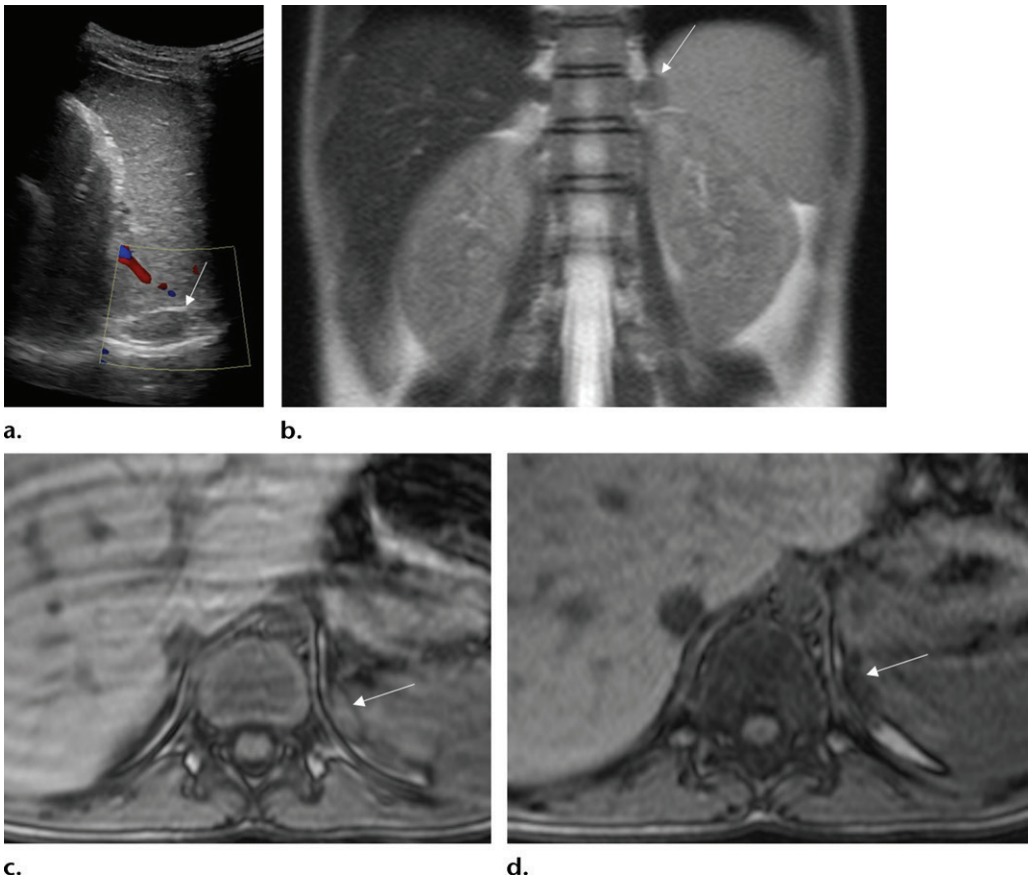

Figure 14. Adrenal adenoma in an 8-year-old girl with abdominal pain. **(a)** Transverse color Doppler US image of the left upper abdomen shows a hypoechoic left suprarenal lesion (arrow) without appreciable internal vascularity. **(b)** Coronal T2-weighted MR image shows an intermediate- to low-signal-intensity left suprarenal mass (arrow). **(c, d)** Axial T1-weighted in-phase **(c)** and out-of-phase **(d)** chemical shift MR images show a left suprarenal lesion (arrows) with signal loss on the out-of-phase image, consistent with intracellular (microscopic) fat.

shift images, due to the presence of microscopic fat (Fig 14c, 14d) (7,17). A signal intensity drop of more than 20% on opposed-phase chemical shift images is highly sensitive and specific for a lipid-rich adenoma (17,30).

Adenomas have variable signal intensity on T1- and T2-weighted MR images (Fig 14b). Rarely, adrenal adenomas may contain foci of hemorrhage and cystic degeneration (15). It is difficult to distinguish larger lipid-poor adenomas from adrenocortical carcinomas at imaging, although carcinomas are typically larger and more heterogeneous and have more frequent calcifications than adenomas (57).

Surgical resection is the curative treatment for functionally active adrenal adenomas (56).

Extralobar Sequestration

A pulmonary sequestration is a type of bronchopulmonary foregut malformation caused by the abnormal development of a portion of the bronchial tree and proximal gastrointestinal tract (59). It is a congenital mass of nonfunctioning lung tissue that has no communication with the tracheobronchial tree. There is anomalous arterial blood supply, typically from the aorta. In intralobar sequestration, there is pulmonary venous return.

In extralobar sequestration, the venous return is usually systemic via the azygos, hemiazygos, or portal venous system. An extralobar sequestration has its own pleural covering if it is in the lung. It is usually located in the left lower lobe, but it can be infradiaphragmatic in 8%–10% of cases (60). In more than 50% of patients, there are other associated anomalies, such as diaphragmatic hernia (most common), diaphragm eventration, hydrops, and vertebral or cardiac malformations (61). Eighty percent of extralobar sequestrations are found in boys (62). It is often diagnosed in the second trimester at prenatal US or fetal MR imaging. Histologic analysis shows dilated and tortuous lung tissue, including bronchioles, alveolar ducts, and alveoli. Dilated lymphatic vessels are also common.

Infradiaphragmatic extralobar sequestration may mimic an adrenal mass at imaging. Suprarenal extralobar sequestration may be seen as a well-defined radiopacity in the upper paraspinal

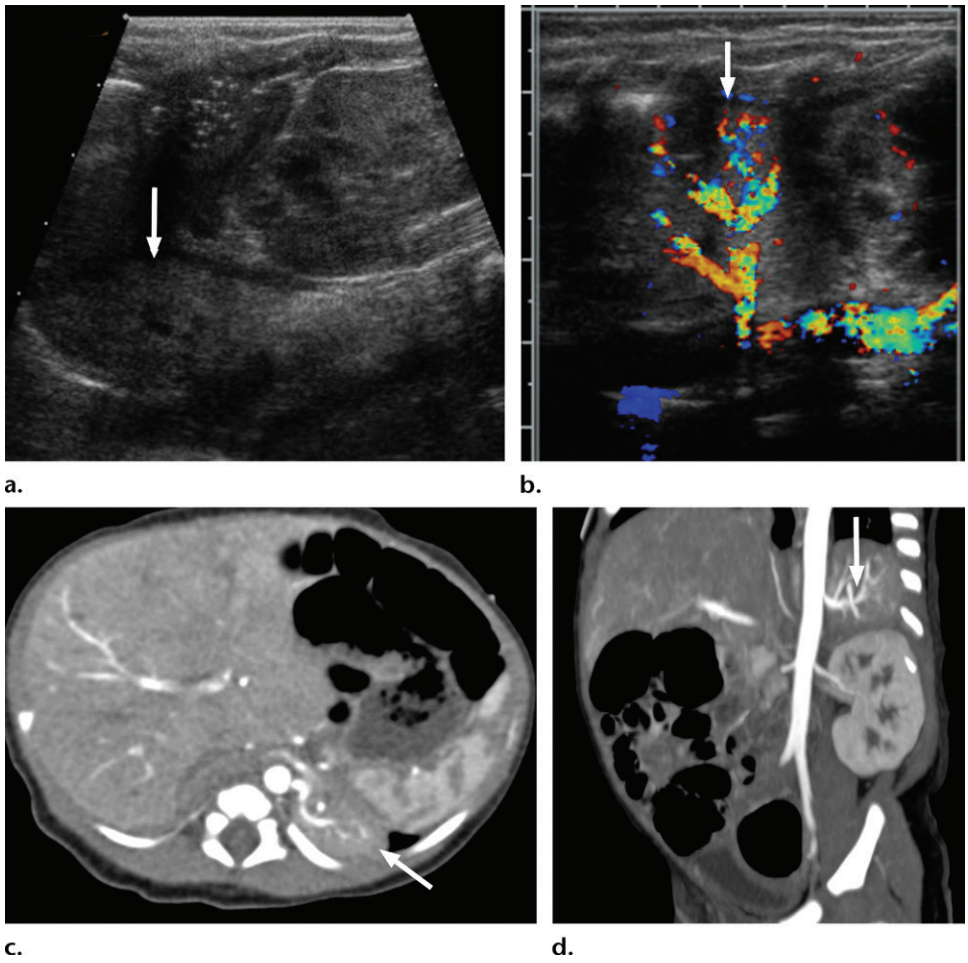

Figure 15. Extralobar sequestration in a 1-day-old girl with abnormal prenatal US findings. **(a, b)** Longitudinal gray-scale **(a)** and color Doppler **(b)** US images of the left upper quadrant show a heterogeneous and predominantly hypoechoic lesion (arrow) in the left suprarenal region, supplied by an artery arising from the aorta. **(c, d)** Axial **(c)** and coronal oblique multiplanar reconstructed **(d)** contrast-enhanced CT images of the abdomen show an enhancing left suprarenal lesion (arrow) that is supplied by an artery arising from the aorta, consistent with extralobar sequestration.

region on chest and abdominal radiographs. US demonstrates a heterogeneous suprarenal mass, often pyramidal (Fig 15a). The increased echogenicity is related to multiple tissue interfaces within the lesion (60). A thin and highly echogenic rim around the lesion may also be seen (63). The blood supply is from the aorta or branches of the aorta. Color and spectral Doppler US is a valuable tool to use in conjunction with gray-scale US to visualize the feeding vessel and to help confirm the diagnosis (Fig 15b). A normal adrenal gland may be seen adjacent to the sequestration, displaced anteriorly.

CT and MR images demonstrate excellent spatial resolution and typically show an enhancing soft-tissue mass in the left suprarenal space (Fig 15c, 15d) (17). The systemic vascular supply is typically well delineated on both CT and MR images (Fig 15d) (64). The differential diagnosis includes neuroblastoma, adrenal hemorrhage, teratoma, and foregut duplication lesions.

The treatment is surgical resection. If the lesion is solitary, the prognosis is excellent.

Extramedullary Hematopoiesis

Extramedullary hematopoiesis (EMH) is defined as the production of blood cells outside normal bone marrow. It is most commonly seen in chronic hemolytic anemias such as thalassemia, sickle cell anemia, and hereditary spherocytosis, as well as in lymphoma and leukemia (17). EMH is less common in children than adults, and it is most commonly seen in adolescents (65). In most patients, EMH is usually asymptomatic; however, patients may present with symptoms secondary to mass effect (65,66). In the abdomen, EMH may be seen involving the perirenal space, kidney, and adrenal gland (17,65).

At imaging, EMH in the paravertebral and perirenal regions may mimic adrenal lesions (17). CT images show well-defined heterogeneous paravertebral masses, which are iso- to hypoat-

RadioGraphics

tenuating to the muscle and may or may not contain internal fat attenuation (66,67). These masses are usually bilateral at multiple levels in a nearly symmetric fashion and do not cause osseous erosions. At MR imaging, EMH appears as a heterogeneous mass with variable signal intensity on T1- and T2-weighted images and variable enhancement (67). Internal macroscopic fatty components show hyperintense signal on T1- and T2-weighted images (17,67). EMH shows increased tracer uptake at technetium 99m–labeled sulfur colloid scintigraphy, confirming the presence of marrow elements.

Conclusion

In this article, we have emphasized the key clinical features and imaging characteristics of nonmalignant adrenal lesions in the pediatric population. Knowledge of the imaging and clinical features of nonmalignant adrenal lesions is helpful to distinguish these lesions from malignant adrenal neoplasms and to guide appropriate management.

References

1. van Vuuren SH, Damen-Elias HA, Stigter RH, et al. Size and volume charts of fetal kidney, renal pelvis, and adrenal gland. Ultrasound Obstet Gynecol 2012;40(6):659–664.
2. Kangarloo H, Diament MJ, Gold RH, et al. Sonography of adrenal glands in neonates and children: changes in appearance with age. J Clin Ultrasound 1986;14(1):43–47.
3. Westra SJ, Zaninovic AC, Hall TR, Kangarloo H, Boechat MI. Imaging of the adrenal gland in children. RadioGraphics 1994;14(6):1323–1340.
4. Schultz CL, Haaga JR, Fletcher BD, Alfidi RJ, Schultz MA. Magnetic resonance imaging of the adrenal glands: a comparison with computed tomography. AJR Am J Roentgenol 1984;143(6):1235–1240.
5. Wasnik AP, Mazza MB, Lalchandani UR, Liu PS. Normal and variant abdominal anatomy on magnetic resonance imaging. Magn Reson Imaging Clin N Am 2011;19(3):521–545, viii.
6. Hoffman CK, Filly RA, Callen PW. The "lying down" adrenal sign: a sonographic indicator of renal agenesis or ectopia in fetuses and neonates. J Ultrasound Med 1992;11(10):533–536.
7. Paterson A. Adrenal pathology in childhood: a spectrum of disease. Eur Radiol 2002;12(10):2491–2508.
8. Strouse PJ, Haller JO, Berdon WE, Rosovsky MA, Bellah RD, Barr M Jr. Horseshoe adrenal gland in association with asplenia: presentation of six new cases and review of the literature. Pediatr Radiol 2002;32(11):778–782.
9. Ditkofsky N, Bradley N, Jeon P. Horseshoe adrenal gland: a rare congenital anomaly. Surg Radiol Anat 2013;35(8):749–754.
10. Siegel MJ, Herman TE. Special imaging casebook. Neonate with osteogenesis imperfecta and asplenia syndrome with horseshoe adrenal. J Perinatol 1999;19(7):543–545.
11. Rozenblit A, Morehouse HT, Amis ES Jr. Cystic adrenal lesions: CT features. Radiology 1996;201(2):541–548.
12. Abeshouse GA, Goldstein RB, Abeshouse BS. Adrenal cysts: review of the literature and report of three cases. J Urol 1959;81(6):711–719.
13. Furihata M, Iida Y, Furihata T, Ito E. A giant lymphatic cyst of the adrenal gland: report of a rare case and review of the literature. Int Surg 2015;100(1):2–8.
14. Balassy C, Navarro OM, Daneman A. Adrenal masses in children. Radiol Clin North Am 2011;49(4):711–727, vi.
15. Elsayes KM, Mukundan G, Narra VR, et al. Adrenal masses: MR imaging features with pathologic correlation. RadioGraphics 2004;24(suppl 1):S73–S86.
16. Barron SH, Emanuel B. Adrenal cyst: a case report and a review of the pediatric literature. J Pediatr 1961;59:592–599.
17. Bittman ME, Lee EY, Restrepo R, Eisenberg RL. Focal adrenal lesions in pediatric patients. AJR Am J Roentgenol 2013;200(6):W542–W556.
18. Sakamoto I, Nakahara N, Fukuda T, Nagayoshi K, Matsunaga N, Hayashi K. Atypical appearance of adrenal pseudocysts. J Urol 1994;152(1):150–152.
19. Vézina CT, McLoughlin MJ, St Louis EL, Gray RR, Bird BL, Wise DJ. Cystic lesions of the adrenals: diagnosis and management. J Can Assoc Radiol 1984;35(2):107–112.
20. Lee MJ, Mayo-Smith WW, Hahn PF, et al. State-of-the-art MR imaging of the adrenal gland. RadioGraphics 1994;14(5):1015–1029; discussion 1029–1032.
21. Goodman SN. Neuroblastoma screening data: an epidemiologic analysis. Am J Dis Child 1991;145(12):1415–1422.
22. Kawashima A, Sandler CM, Ernst RD, et al. Imaging of nontraumatic hemorrhage of the adrenal gland. RadioGraphics 1999;19(4):949–963.
23. Iuchtman M, Breitgand A. Traumatic adrenal hemorrhage in children: an indicator of visceral injury. Pediatr Surg Int 2000;16(8):586–588.
24. Adem PV, Montgomery CP, Husain AN, et al. Staphylococcus aureus sepsis and the Waterhouse-Friderichsen syndrome in children. N Engl J Med 2005;353(12):1245–1251.
25. Dunnick NR. Hanson lecture. Adrenal imaging: current status. AJR Am J Roentgenol 1990;154(5):927–936.
26. Cohen EK, Daneman A, Stringer DA, Soto G, Thorner P. Focal adrenal hemorrhage: a new US appearance. Radiology 1986;161(3):631–633.
27. Atkinson GO Jr, Zaatari GS, Lorenzo RL, Gay BB Jr, Garvin AJ. Cystic neuroblastoma in infants: radiographic and pathologic features. AJR Am J Roentgenol 1986;146(1):113–117.
28. Deeg KH, Bettendorf U, Hofmann V. Differential diagnosis of neonatal adrenal haemorrhage and congenital neuroblastoma by colour coded Doppler sonography and power Doppler sonography. Eur J Pediatr 1998;157(4):294–297.
29. Jordan E, Poder L, Courtier J, Sai V, Jung A, Coakley FV. Imaging of nontraumatic adrenal hemorrhage. AJR Am J Roentgenol 2012;199(1):W91–W98.
30. Elsayes KM, Emad-Eldin S, Morani AC, Jensen CT. Practical approach to adrenal imaging. Radiol Clin North Am 2017;55(2):279–301.
31. Fulcher AS, Das Narla L, Hingsbergen EA. Pediatric case of the day. Wolman disease: primary familial xanthomatosis with involvement and calcification of the adrenal glands. RadioGraphics 1998;18(2):533–535.
32. Chung EM, Biko DM, Schroeder JW, Cube R, Conran RM. From the radiologic pathology archives. Precocious puberty: radiologic-pathologic correlation. RadioGraphics 2012;32(7):2071–2099.
33. Lambert SM, Vilain EJ, Kolon TF. A practical approach to ambiguous genitalia in the newborn period. Urol Clin North Am 2010;37(2):195–205.
34. Chavhan GB, Parra DA, Oudjhane K, Miller SF, Babyn PS, Pippi Salle FL. Imaging of ambiguous genitalia: classification and diagnostic approach. RadioGraphics 2008;28(7):1891–1904.
35. Hernanz-Schulman M, Brock JW 3rd, Russell W. Sonographic findings in infants with congenital adrenal hyperplasia. Pediatr Radiol 2002;32(2):130–137.
36. Al-Alwan I, Navarro O, Daneman D, Daneman A. Clinical utility of adrenal ultrasonography in the diagnosis of congenital adrenal hyperplasia. J Pediatr 1999;135(1):71–75.
37. Sivit CJ, Hung W, Taylor GA, Catena LM, Brown-Jones C, Kushner DC. Sonography in neonatal congenital adrenal hyperplasia. AJR Am J Roentgenol 1991;156(1):141–143.
38. Stikkelbroeck NM, Suliman HM, Otten BJ, Hermus AR, Blickman JG, Jager GJ. Testicular adrenal rest tumours in postpubertal males with congenital adrenal hyperplasia: sonographic and MR features. Eur Radiol 2003;13(7):1597–1603.
39. Avila NA, Premkumar A, Merke DP. Testicular adrenal rest tissue in congenital adrenal hyperplasia: comparison of MR imaging and sonographic findings. AJR Am J Roentgenol 1999;172(4):1003–1006.
40. Havekes B, Romijn JA, Eisenhofer G, Adams K, Pacak K. Update on pediatric pheochromocytoma. Pediatr Nephrol 2009;24(5):943–950.

41. Ross JH. Pheochromocytoma: special considerations in children. Urol Clin North Am 2000;27(3):393–402.
42. Jasperson KW, Kohlmann W, Gammon A, et al. Role of rapid sequence whole-body MRI screening in SDH-associated hereditary paraganglioma families. Fam Cancer 2014;13(2):257–265.
43. Ciftci AO, Tanyel FC, Senocak ME, Büyükpamukçu N. Pheochromocytoma in children. J Pediatr Surg 2001;36(3):447–452.
44. McHugh K. Renal and adrenal tumours in children. Cancer Imaging 2007;7:41–51.
45. Stowens D. Neuroblastoma and related tumors. AMA Arch Pathol 1957;63(5):451–459.
46. Lonergan GJ, Schwab CM, Suarez ES, Carlson CL. Neuroblastoma, ganglioneuroblastoma, and ganglioneuroma: radiologic-pathologic correlation. RadioGraphics 2002;22(4):911–934.
47. Scherer A, Niehues T, Engelbrecht V, Mödder U. Imaging diagnosis of retroperitoneal ganglioneuroma in childhood. Pediatr Radiol 2001;31(2):106–110.
48. Geoerger B, Hero B, Harms D, Grebe J, Scheidhauer K, Berthold F. Metabolic activity and clinical features of primary ganglioneuromas. Cancer 2001;91(10):1905–1913.
49. Lucas K, Gula MJ, Knisely AS, Virgi MA, Wollman M, Blatt J. Catecholamine metabolites in ganglioneuroma. Med Pediatr Oncol 1994;22(4):240–243.
50. Jasinski RW, Samuels BI, Silver TM. Sonographic features of retroperitoneal ganglioneuroma. J Ultrasound Med 1984;3(9):413–415.
51. Daneman A, Baunin C, Lobo E, et al. Disappearing suprarenal masses in fetuses and infants. Pediatr Radiol 1997;27(8):675–681.
52. Ichikawa T, Ohtomo K, Araki T, et al. Ganglioneuroma: computed tomography and magnetic resonance features. Br J Radiol 1996;69(818):114–121.
53. Rajiah P, Sinha R, Cuevas C, Dubinsky TJ, Bush WH Jr, Kolokythas O. Imaging of uncommon retroperitoneal masses. RadioGraphics 2011;31(4):949–976.
54. Lloyd RV. Adrenal cortical tumors, pheochromocytomas and paragangliomas. Mod Pathol 2011;24(suppl 2):S58–S65.
55. Wieneke JA, Thompson LD, Heffess CS. Adrenal cortical neoplasms in the pediatric population: a clinicopathologic and immunophenotypic analysis of 83 patients. Am J Surg Pathol 2003;27(7):867–881.
56. Hanna AM, Pham TH, Askegard-Giesmann JR, et al. Outcome of adrenocortical tumors in children. J Pediatr Surg 2008;43(5):843–849.
57. Flynt KA, Dillman JR, Davenport MS, et al. Pediatric adrenocortical neoplasms: can imaging reliably discriminate adenomas from carcinomas? Pediatr Radiol 2015;45(8):1160–1168.
58. Agrons GA, Lonergan GJ, Dickey GE, Perez-Monte JE. Adrenocortical neoplasms in children: radiologic-pathologic correlation. RadioGraphics 1999;19(4):989–1008.
59. Heithoff KB, Sane SM, Williams HJ, et al. Bronchopulmonary foregut malformations: a unifying etiological concept. AJR Am J Roentgenol 1976;126(1):46–55.
60. Pumberger W, Moroder W, Wiesbauer P. Intraabdominal extralobar pulmonary sequestration exhibiting cystic adenomatoid malformation: prenatal diagnosis and characterization of a left suprarenal mass in the newborn. Abdom Imaging 2001;26(1):28–31.
61. White J, Chan YF, Neuberger S, Wilson T. Prenatal sonographic detection of intra-abdominal extralobar pulmonary sequestration: report of three cases and literature review. Prenat Diagn 1994;14(8):653–658.
62. Corbett HJ, Humphrey GM. Pulmonary sequestration. Paediatr Respir Rev 2004;5(1):59–68.
63. Rosado-de-Christenson ML, Frazier AA, Stocker JT, Templeton PA. From the archives of the AFIP. Extralobar sequestration: radiologic-pathologic correlation. RadioGraphics 1993;13(2):425–441.
64. Felker RE, Tonkin IL. Imaging of pulmonary sequestration. AJR Am J Roentgenol 1990;154(2):241–249.
65. Zhu G, Wu X, Zhang X, Wu M, Zeng Q, Li X. Clinical and imaging findings in thalassemia patients with extramedullary hematopoiesis. Clin Imaging 2012;36(5):475–482.
66. Ginzel AW, Kransdorf MJ, Peterson JJ, Garner HW, Murphey MD. Mass-like extramedullary hematopoiesis: imaging features. Skeletal Radiol 2012;41(8):911–916.
67. Roberts AS, Shetty AS, Mellnick VM, Pickhardt PJ, Bhalla S, Menias CO. Extramedullary haematopoiesis: radiological imaging features. Clin Radiol 2016;71(9):807–814.